Analytical and Bioanalytical Chemistry (2021) 413:7081–7091
https://doi.org/10.1007/s00216-021-03677-x

RESEARCH PAPER

Development of a DNAzyme-based colorimetric biosensor assay for dual detection of Cd^{2+} and Hg^{2+}

Dawei Li[1] · Shen Ling[1] · Xinru Cheng[1] · Zhaoqi Yang[3] · Bei Lv[2]

Received: 19 July 2021 / Revised: 15 September 2021 / Accepted: 17 September 2021 / Published online: 29 September 2021

Abstract

A colorimetric biosensor assay has been developed for Cd^{2+} and Hg^{2+} detection based on Cd^{2+}-dependent DNAzyme cleavage and Hg^{2+}-binding-induced conformational switching of the G-quadruplex fragment. Two types of multifunctional magnetic beads (Cd-MBs and Hg-MBs) were synthesized by immobilizing two functionalized DNA sequences on magnetic beads via avidin-biotin chemistry. For Cd^{2+} detection, Cd-MBs are used as recognition probes, which are modified with a single phosphorothioate ribonucleobase (rA) substrate (PS substrate) and a Cd^{2+}-specific DNAzyme (Cdzyme). In the presence of Cd^{2+}, the PS substrate is cleaved by Cdzyme, and single-stranded DNA is released as the signal transduction sequence. After molecular assembly with the other two oligonucleotides, duplex DNA is produced, and it can be recognized and cleaved by FokI endonuclease. Thus, a signal output component consisting of a G-quadruplex fragment is released, which catalyzes the oxidation of ABTS with the addition of hemin and H_2O_2, inducing a remarkably amplified colorimetric signal. To rule out false-positive results and reduce interference signals, Hg-MBs modified with poly-T fragments were used as Hg^{2+} accumulation probes during the course of Cd^{2+} detection. On the other hand, Hg-MBs can perform their second function in Hg^{2+} detection by changing the catalytic activity of the G-quadruplex/hemin DNAzyme. In the presence of Hg^{2+}, the G-quadruplex structure in Hg-MBs is disrupted upon Hg^{2+} binding. In the absence of Hg^{2+}, an intensified color change can be observed by the naked eye for the formation of intact G-quadruplex/hemin DNAzymes. The biosensor assay exhibits excellent selectivity and high sensitivity. The detection limits for Cd^{2+} and Hg^{2+} are 1.9 nM and 19.5 nM, respectively. Moreover, the constructed sensors were used to detect environmental water samples, and the results indicate that the detection system is reliable and could be further used in environmental monitoring. The design strategy reported in this study could broadly extend the application of metal ion-specific DNAzyme-based biosensors.

Keywords DNAzyme · Aptamer · Cadmium · Mercury · Biosensor

Introduction

Heavy metal pollution causes severe damage to the ecosystem and compromises food safety and human health [1, 2]. Cadmium ions (Cd^{2+}), for example, are highly toxic metal ions with biological half-lives in the range of 10–30 years [3]. Cadmium can accumulate in tissues and organisms and causes slow growth, nephrotoxicity, liver functional dysfunction, bone demineralization, and anemia by inhibiting or interfering with the abortion of the necessary iron, calcium, or zinc for alkaline cells to perform physiological functions [4]. Cadmium has also been classified as a cancerogen by the International Agency for Research on Cancer (IARC) [5]. Mercury ions (Hg^{2+}) can also cause cytotoxic and genotoxic effects in human cell lines [6], leading to severe damage to various organs, such as the brain and kidneys and

Dawei Li and Shen Ling contributed equally to this work.

✉ Dawei Li
dwli@njfu.edu.cn

✉ Bei Lv
lvbei@jssnu.edu.cn

[1] Co-Innovation Center for Sustainable Forestry in Southern China, Key Laboratory of Forest Genetics & Biotechnology, Ministry of Education, College of Biology and the Environment, Nanjing Forestry University, Nanjing 210037, China

[2] Jiangsu Key Laboratory for Biofunctional Molecules, College of Life Science and Chemistry, Jiangsu Second Normal University, Nanjing 210013, China

[3] School of Pharmaceutical Sciences, Jiangnan University, Wuxi 214122, China

cardiovascular systems, at very low concentrations [7]. Inductively coupled plasma-mass spectrometry (ICP-MS) [8] and atomic absorption/fluorescence spectrometry [9] are widely used methods for heavy metal ion detection with high selectivity and sensitivity. However, these techniques often require expensive analytical instrumentation, complicated sample preparation and testing processes, long operation times, and skilled technicians, sometimes with a high false-positive rate, which limits their wide applications for routine testing. Therefore, it is of great significance to establish an efficient and rapid method for the determination of heavy metal ions.

With the rapid development of functional nucleic acid molecules, the emergence of aptamer- and DNAzyme-based biosensors has provided new molecular detection methods for ions, small molecules, peptides, and even cells [10]. Aptamers are short single-stranded oligonucleotides that are versatilely used as recognition probes because of their high affinity and specificity for target molecules [11]. Many aptamer-based biosensors have been developed for the detection of Cd^{2+} [12], Hg^{2+} [13], Pb^{2+} [14], Ag^{+} [15], and As^{3+} [16]. On the other hand, DNAzymes have also been widely used as target recognition elements in mental ion sensing applications due to their short detection time, high sensitivity, and excellent accuracy. To date, many DNAzymes have been identified and used for metal ion detection, such as Zn^{2+} [17], Pb^{2+} [18], Na^{+} [19], UO_2^{2+} [20], Mg^{2+} [21], Ag^{+} [22], Ca^{2+} [23], Cu^{2+} [24], Cr^{3+} [25], Cd^{2+} [26], and Hg^{2+} [27].

Liu and coworkers selected specific DNAzymes toward Cd^{2+}, which were further used for Cd^{2+} detection through fluorescence spectrometry [26]. In this study, single phosphorothioate (PS)-modified ribonucleobase (rA)-containing DNA was used as the substrate, and a highly specific DNAzyme named BN-Cd16 with only 12 nucleotides in the catalytic loop was isolated in vitro. Compared with another DNAzyme, Ce13d, which was reported earlier [28], BN-Cd16 is most active with Cd^{2+} and exhibits higher selectivity when using a PS substrate. However, BN-Cd16 still shows moderate activity with some thiophilic heavy metal ions, such as Hg^{2+} [29, 30], which may produce interference signals when BN-Cd16 is used as the recognition component in Cd^{2+}-specific biosensor construction.

Herein, we report a DNAzyme-based colorimetric biosensor assay that is used to detect Cd^{2+} and Hg^{2+}. In our system, Cd-MBs modified with a PS substrate and Cd^{2+}-specific DNAzyme (BN-Cd16) were employed as recognition probes for Cd^{2+} detection, and a DNAzyme G-quadruplex fragment was used to produce a colorimetric signal. To rule out false-positive results induced by Hg^{2+}-induced nonspecific substrate cleavage, Hg-MBs modified with the poly-T fragment were used for Hg^{2+} accumulation and separation during Cd^{2+} detection. For Hg^{2+} detection, Hg-MBs perform their second function, which is a response to Hg^{2+} binding through the formation or disintegration of the intact G-quadruplex/hemin DNAzyme [31], leading to an intensified color change. The constructed biosensor system exhibits excellent selectivity and high sensitivity. Furthermore, the sensors were used to detect environmental water samples, and the target recovery results were reasonable, indicating that the sensor system is reliable and could be further used in environmental monitoring.

Materials and methods

Materials

All oligonucleotides were provided by Sangon Biotech (Shanghai, China) with HPLC purification. The sequences of oligonucleotides are given in the ESM, Table S1. Beaver Beads™ Streptavidin (1 μm in average diameter) was purchased from Beaver (Suzhou, China). FokI exonuclease was purchased from Takara Bio, Inc. (Dalian, China). ABTS, hemin, HEPES, MES, PBS, and PBST were purchased from Sangon Biotech (Shanghai, China). The metal salts were obtained from Sigma Aldrich Co., Ltd. (Shanghai, China). All buffers and solutions were prepared with deionized (DI) water (Milli-Q Plus system, with a resistivity of 18.2 ΩM cm).

Preparation of Cd-MBs and Hg-MBs

First, 40 μL of 10 mg/mLstreptavidin-coupled magnetic beads (MBs) was washed three times with 1× PBST buffer (136.89 mM NaCl, 2.67 mM KCl, 8.1 mM Na_2HPO_4, 1.76 mM KH_2PO_4, 0.05% (*w*/*v*) Tween-20, pH = 7.4). Then, MBs was diluted with 200 μL PBST buffer. Ten microliters of PS substrate (100 μM) and 10 μL of Cdzyme (100 μM) were added to 80 μL of PBS buffer solution (136.89 mM NaCl, 2.67 mM KCl, 8.1 mM Na_2HPO_4, 1.76 mM KH_2PO_4, pH = 7.4). The mixed solution was annealed by heating to 90 °C for 2 min and then slowly cooled to room temperature. Then, 20 μL of the above solution was added to 100 μL of MB solution and mixed well at room temperature for 30 min to produce Cd-MBs. AT11A was diluted and annealed in CB1 buffer (25 mM HEPES, 20 mM KCl, 200 mM NaCl, 0.025% (*w*/*v*) Triton X-100, pH 5.3) to a concentration of 10 μM. Then, 20 μL of the above solution was added to 100 μL of MB solution and mixed well at room temperature for 30 min to produce Hg-MBs. The DNA concentrations before and after MB treatment were measured with a BioDrop (Cambridge, UK) to ensure the efficient immobilization of biotin-modified DNA on the MBs, as shown in the ESM, Table S2. The Cd-MBs and Hg-MBs were then washed three times with PBST buffer to remove excess biotin–ssDNA. Finally, Cd-MBs and Hg-MBs were resuspended in 50 μL of the buffer solutions.

Sensing protocol

For Cd^{2+} detection, to remove the possible Hg^{2+} contamination that may induce non-Cd^{2+}-specific substrate cleavage and false-positive results, 5 μL of sample solution was mixed with 20 μL of Hg-MB solution in CB1 buffer to a final volume of 30 μL and incubated at room temperature with gentle shaking for 10 min. Then, the solution was separated with a magnetic rack, and the supernatant was transferred into a new centrifuge tube. Then, the above solutions containing different concentrations of Cd^{2+} and 10 μL of Cd-MB solution were mixed well in CT1 buffer (50 mM MES, 25 mM NaCl, pH 6.0) to a final volume of 50 μL and incubated at room temperature for 20 min. Each solution was then separated with a magnetic rack, and the supernatant was transferred into a new centrifuge tube. After that, the above supernatant was added to a solution containing 200 nM OD-2 and OD-3 complex (annealed in 25 mM tris-HCl, 100 mM NaCl, pH 7.3), 2.5 U FokI endonuclease in 1× reaction buffer (50 mM NaCl, 10 mM Tris-HCl, 10 mM $MgCl_2$, 1 mM dithiothreitol, pH 7.0), and the reaction solution was incubated at 37 °C for 30 min. Then, 70 μL of FokI reaction mixture and 4 μL of 10 μM hemin were mixed in CB2 buffer (25 mM HEPES, 200 mM NaCl, 50 mM KCl, 0.025% Triton X-100, 150 mM NH_4Cl, pH 5.3) to a final volume of 190 μL and kept at room temperature in the dark for 30 min. Finally, 5 μL of 40 mM ABTS and 5 μL of 40 mM H_2O_2 were added to a final volume of 200 μL. The absorption spectrum of the reaction product $ABTS^{\bullet+}$ was recorded after 15 min of reaction with an iMark Absorbance Microplate Reader (Hercules, USA). Absorbance at 415 nm was used for quantitative analysis.

For Hg^{2+} detection, 5 μL of sample solution containing different Hg^{2+} concentrations, 10 μL of Hg-MB solution, and 4 μL of 10 μM hemin were mixed in CB1 buffer to a final volume of 190 μL and incubated at room temperature in the dark with gentle shaking for 30 min. Finally, 5 μL of 40 mM ABTS and 5 μL of 40 mM H_2O_2 were added to a final volume of 200 μL. The absorption spectrum of the reaction product $ABTS^{\bullet+}$ was recorded after 15 min of reaction with an iMark Absorbance Microplate Reader (Hercules, USA). Absorbance at 415 nm was used for quantitative analysis.

To study the effect of pH and anions on the assay, CT2 buffer (50 mM MES, 25 mM NaAc, pH 6.0) was used in the PS-substrate cleavage reaction, while CB3 buffer (25 mM HEPES, 20 mM KAc, 100 mM NaAc, 0.025% (*w*/*v*) Triton X-100, pH 5.3) was used in G-quadruplex-hemin formation. For the test on different pH values, the buffers were adjusted by adding NaOH/HAc. Solutions containing salts with different anions, including Na_2SO_4, $NaNO_3$, NaCl, NaBr, and NaI, were added to metal ion solutions, and the detections were performed in the same way.

To investigate the specificity of the assay, other metal ions, including Mg^{2+}, Ca^{2+}, Ba^{2+}, Mn^{2+}, Ni^{2+}, Co^{2+}, and Zn^{2+}, were tested in the same way.

Gel electrophoresis

The molecular assembly and reaction products were determined by one-dimensional electrophoresis through 1.5% (wt/vol) native PAGE gels run in TBE buffer (90 mM Tris borate/2.5 mM EDTA, pH 8.3) for 2 h at room temperature and stained with GelRed for 45 min. The gel was photographed using a gel documentation system (BioRad ChemiDocXRS, USA).

Results and discussion

Sensing principle

Scheme 1 illustrates the basic principle of the assay for $Cd^{2+}$and Hg^{2+} detection. Cd-MBs and Hg-MBs are two types of multifunctional magnetic beads. In Cd-MBs, Cdzyme hybridizes with a PS substrate that is immobilized on magnetic beads via avidin-biotin chemistry. Cd-MBs are used as recognition probes for Cd^{2+} detection. In the presence of Cd^{2+}, the PS substrate is cleaved at the phosphorothioate-modified ribonucleobase (rA) site due to the catalytic activity of Cdzyme, and single-stranded DNA (OD-1) is released as the signal transduction sequence. After separation with a magnetic rack, OD-1 in the supernatant hybridizes with the OD-2 and OD3 complex to form duplex DNA, in which a FokI recognition site appears. Then, the duplex DNA is cleaved by FokI endonuclease, leading to the release of a G-rich sequence that can further form a G-quadruplex/hemin DNAzyme (see the dashed boxes in Scheme 1). After that, the resulting DNAzyme catalyzes the H_2O_2-mediated oxidation of colorless ABTS to green-colored $ABTS^{\bullet+}$, inducing a colorimetric signal that can be observed by the naked eye.

Although the Cd^{2+}-specific DNAzyme BN-Cd16 used in this study efficiently cleaves PS-substrate DNA, BN-Cd16 still showed moderate activity against other metal ions, such as Hg^{2+} [26]. In addition, strong thiophilicity is an important feature of Hg^{2+}, which leads to cleavage and desulfurization of PS substrates in the presence of Hg^{2+} [30]. Consequently, nonnegligible interference signals may be produced if Cd-MBs are used alone to detect Cd^{2+} in a solution containing both Cd^{2+} and Hg^{2+}. To solve this problem, another multifunctional magnetic bead, Hg-MBs, was designed. In Hg-MBs, the magnetic beads are modified with AT11A, which is a split G-quadruplex fragment containing a Poly-T region. Hg-MBs have two functions. First, it can be used as a Hg^{2+} accumulation prob during the course of Cd^{2+} detection through the formation of thymine–Hg^{2+}–thymine base

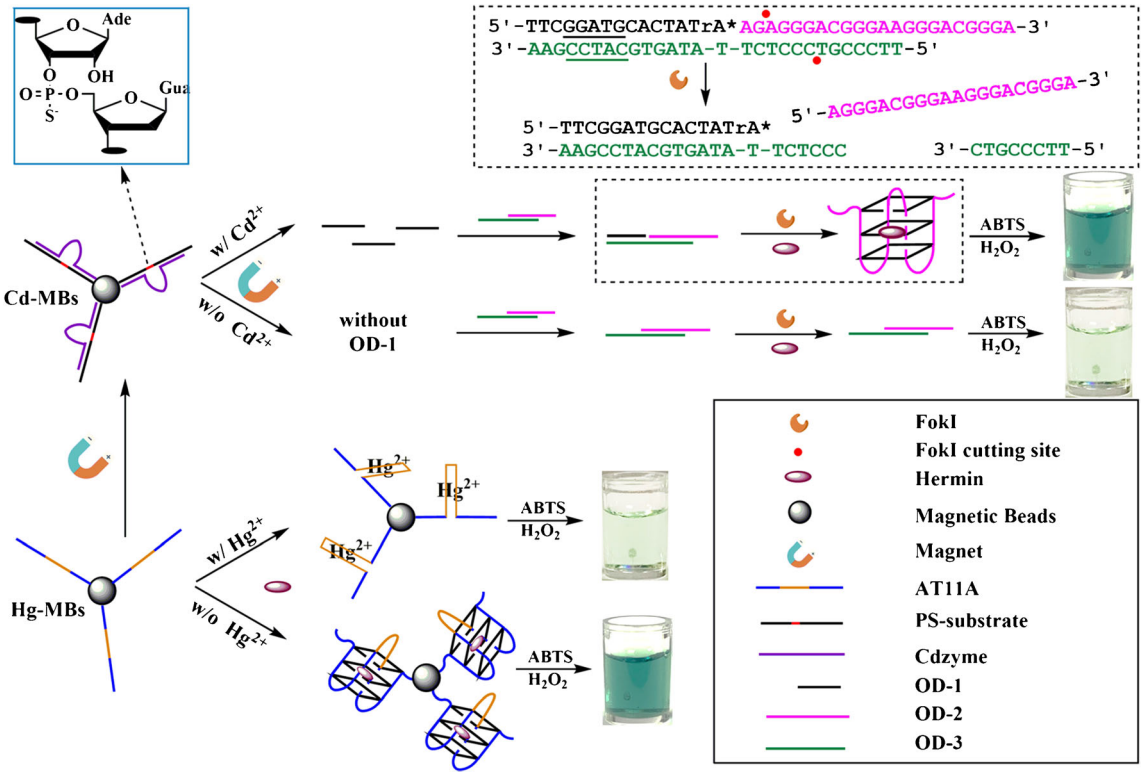

Scheme 1 Schematic illustration of the proposed sensor system for Cd^{2+} and Hg^{2+} detection using multifunctional magnetic beads (Cd-MBs and Hg-MBs). For Cd^{2+} detection, the PS substrate modified in Cd-MBs is cleaved by Cdzyme in the presence of Cd^{2+}, and OD-1 is released. OD-1 hybridizes with OD-2 and OD-3 to form duplex DNA with a FokI recognition site. FokI digestion produces a G-quadruplex that catalyzes the oxidation of ABTS with the addition of hemin and H_2O_2, inducing a remarkable colorimetric signal. Hg-MB treatment and magnetic separation decreased the interference signals induced by Hg^{2+}-induced nonspecific PS-substrate cleavage. For Hg^{2+} detection, G-quadruplex formation is inhibited by the binding of Hg^{2+} in the poly-T region of AT11A in Hg-MBs, leading to a decrease in the peroxidase activity of G-quadruplex/hemin and an intensified color change

pairing. The second function is applied in Hg^{2+} detection. As shown in the lower part of Scheme 1, an intact G-quadruplex/hemin DNAzyme is assembled in the absence of Hg^{2+}, while disintegration of G-quadruplex occurs in the presence of Hg^{2+}, leading to a significant difference in G-quadruplex/hemin DNAzyme activity and an intensified color change.

Optimization of the experimental conditions

It is well known that the structures and peroxidase activity of G-quadruplex-based DNAzymes are highly sensitive to their loop length and composition [32]. According to previous studies, AT11A and OD-2 were chosen as the optimal sequences for their excellent catalytic activity when forming G-quadruplex/hemin DNAzymes [31]. To achieve the best performance for quantitative detection, several other vital experimental conditions were optimized, including the concentration of the OD-2 and OD-3 complex, the amount of FokI endonuclease, and the reaction time of ABTS oxidation. The OD-2 and OD-3 complex can hybridize with the cleavage products (OD-1) of the PS substrate and form duplex DNA. To optimize the concentration of the OD-2 and OD-3 complex, 500 nM Cd^{2+} solution was examined with different OD-2 and OD-3 complex concentrations. As shown in the ESM, Fig. S1A, the absorption intensity increases significantly with increasing OD-2 and OD-3 complex concentration until it reaches 200 nM. Thus, the optimal OD-2 and OD-3 complex concentration is 200 nM. The FokI endonuclease catalyzes duplex DNA cleavage and releases the G-rich sequence. The effect of the amount of FokI was investigated. As shown in the ESM, Fig. S1B, the resultant absorption responses increase with the increased amount of FokI and level off when the enzyme exceeds 2.5 U. Therefore, the amount of FokI endonuclease is set at 2.5 U. Finally, the reaction time of ABTS oxidation is optimized as well. As shown in the ESM, Fig. S1C, the absorption intensity reaches a plateau when the oxidation reaction takes 15 min. Thus, the absorption spectrum of the oxidation reaction product $ABTS^{\bullet+}$ was recorded after 15 min of reaction.

Colorimetric detection of Cd^{2+}

To confirm the effectiveness of our sensor system for Cd^{2+} detection, Cd-MBs were used as probes, and colorimetric signals were measured in Cd^{2+} solutions with different concentrations. As shown in Fig. 1, Cd^{2+}dose-dependently increased

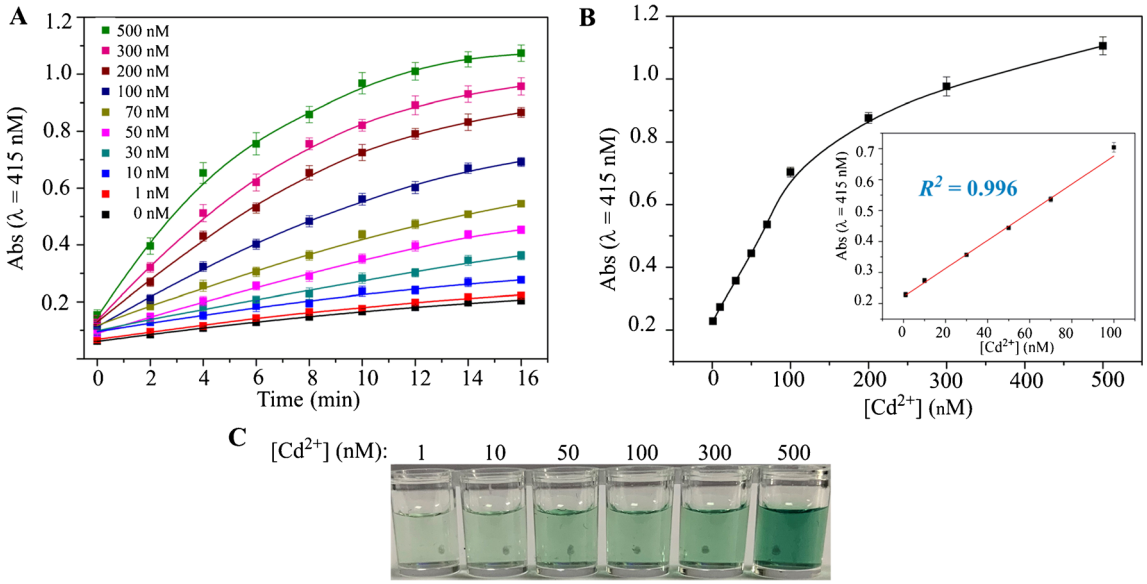

Fig. 1 Colorimetric detection of Cd^{2+} using Hg-MBs. **A** Kinetics of sensor absorbance enhancement with various concentrations of Cd^{2+}. **B** The correlation between the absorbance intensity and the concentration of Cd^{2+}. The absorption intensity at 415 nm of the reaction product $ABTS^{\bullet+}$ was recorded after 15 min and used for quantitative analysis. **C** The color change response to the Cd^{2+} concentration. Data are the means, and error bars show the standard deviation of three repeated experiments

the absorbance intensity (Abs) when plotting the recorded absorbance intensity against the different concentrations of Cd^{2+}. As indicated in Fig. 1B, the Ab values significantly increased in the range of 1 to 100 nM and tended to be gentle when the Cd^{2+} concentration exceeded 100 nM. The inset of Fig. 1B shows a good linear relationship between the absorbance response and the Cd^{2+} concentration, and the range is 1 to 100 nM. The linear equation is Abs = 0.221 + 0.00455C_{Cd} (C_{Cd} is the Cd^{2+} concentration). The correlation coefficient of the linear regression equation (R^2) is 0.996. The limit of detection (LOD) is estimated to be 1.9 nM (signal-to-noise ratio of 3). According to the U.S. Environmental Protection Agency (EPA), the maximal contamination level in drinking water is 5 μg/L(45 nM) Cd^{2+}, which is in the linear range of our designed sensor system. In addition, obvious color changes can be observed with increasing Cd^{2+} concentration due to the enhancement of G-quadruplex/hemin catalytic activity and the oxidation of colorless ABTS to green-colored $ABTS^{\bullet+}$, as shown in Fig. 1C. In addition, to further confirm the feasibility of the assay, some control experiments were performed. As shown in the ESM, Fig. S2, negligible absorbance was recorded in the absence of Cdzyme, OD-2, FokI, or hemin, indicating that the observed strong absorbance was indeed triggered by the synergistic effect of Cdzyme-mediated PS-substrate cleavage, FokI digestion, and oxidation of ABTS catalyzed by the peroxidase activity of G-quadruplex/hemin.

To verify the accuracy and reliability of our Cd^{2+} detection sensor in a Hg^{2+} contamination solution, 50 nM Hg^{2+} was added to the Cd^{2+} standard samples, and Cd^{2+} concentrations were determined with our sensor system. All the samples were divided into two groups. Group A contained Cd^{2+} solutions at different concentrations, while group B was obtained by the addition of 100 nM Hg^{2+} to each sample of group A. Before detection, all samples were treated with Hg-MBs to remove the potential Hg^{2+} contamination that may lead to nonspecific PS-substrate cleavage. Based on the calibration curves from our absorption assay (Fig. 1B), the Cd^{2+} concentration in each sample was calculated. The quantitative results are described in Table 1 and were compared by Student's *t* test. The *t* values do not exceed the theoretical value at the 95% confidence level, which implies that the Cd^{2+} concentrations detected from the two groups of samples are not significantly different. These results confirm the accuracy of our Cd^{2+} detection sensor and can be used in samples with Hg^{2+} contamination. According to the above results, the Cd^{2+} detection sensor reported in this work is comparable with the previously reported DNAzyme-based Cd^{2+} detection sensors (see ESM, Table S3 for details), and it could have better Cd^{2+} response specificity, especially in Hg^{2+} contamination solutions.

DNA structures and product confirmation with gel electrophoresis

To further confirm that the observed color change and absorbance increase were indeed caused by Cd^{2+}-specific DNAzyme (Cdzyme)-mediated PS substrate cleavage and subsequent molecular assembly of DNA strands and FokI digestion (see Scheme 1), native polyacrylamide gel electrophoresis was used to identify the molecular structural changes during those steps. As shown in the ESM, Fig. S3A, the cleaved products (OD-1) accumulated when the Cd^{2+}

Table 1 Cd^{2+} determination by the proposed method in two groups of samples (n = 6)

Group	Sample	Cd^{2+} added (nM)	Hg^{2+} added (nM)	Cd^{2+} detected (nM)	t	RSD (%)
A	A1	30.00	–	29.97	1.79	0.63
B	B1	30.00	50.00	30.41		1.90
A	A2	50.00	–	49.84	2.31	0.40
B	B2	50.00	50.00	50.39		1.10
A	A3	70.00	–	70.04	1.04	0.85
B	B3	70.00	50.00	70.43		1.15

Theoretical t (5, 95%) = 2.571

RSD represents the standard deviation of six repetitive measurements

concentration was increased. Figure S3B in the ESM shows the formation of a DNA complex through the molecular assembly of OD-1, OD-2, and OD-3. In addition, we examined whether the FokI digestion product, a G-rich strand, responds to the Cd^{2+} concentration. As shown in the ESM, Fig. S3C, the G-rich strands digested by FokI endonuclease positively responded to the increase in Cd^{2+} concentrations, which confirms that the signal transduction pathway is consistent with our design strategy, as shown in Scheme 1.

Colorimetric detection of Hg^{2+}

To verify the feasibility of the designed sensor system for Hg^{2+} detection, Hg-MBs were used as recognition probes, and colorimetric detection was performed. As shown in Fig. 2, Hg^{2+} solutions with different concentrations were measured under the experimental conditions. In the absence of Hg^{2+}, an intact G-quadruplex structure could accommodate hemin, leading to the enhancement of its catalytic activity and the oxidation of colorless ABTS to green-colored $ABTS^{\bullet+}$. With increasing Hg^{2+} concentration, the peroxidase activity of G-quadruplex/hemin decreased, resulting in lower UV absorbance at 415 nm (Fig. 2A) and distinct color changes (Fig. 2C). The correlation between the absorbance intensity (Abs) and the Hg^{2+} concentration was measured in the range from 0 to 2000 nM and is shown in Fig. 2B. The inset of Fig. 2B shows a linear relationship between the absorbance response and Hg^{2+} concentration, and the range is 0 to 400 nM. The linear equation is Abs = 1.048–0.002C_{Hg} (C_{Hg} is the Hg^{2+} concentration). The correlation coefficient of the linear regression equation (R^2) is 0.983. The Hg-MBs could provide a clear readout for

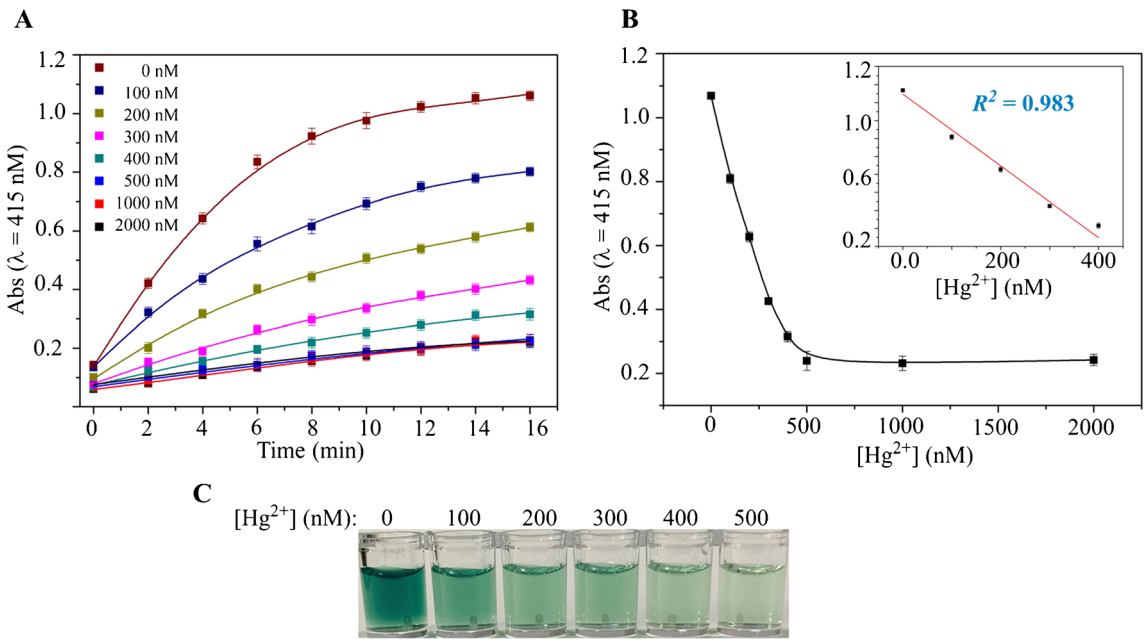

Fig. 2 Colorimetric detection of Hg^{2+} using Hg-MBs. **A** Kinetics of sensor absorbance with various concentrations of Hg^{2+}. **B** The correlation between the absorbance intensity and the concentration of Hg^{2+}. The absorption intensity at 415 nm of the reaction product $ABTS^{\bullet+}$ was recorded after 15 min and used for quantitative analysis. **C** The color change response to Hg^{2+} concentration. Data are the means, and error bars show the standard deviation of three repeated experiments

the presence of Hg^{2+} at concentrations as low as 19.5 nM, where the limit of detection (LOD) was defined based on a signal-to-noise ratio of 3. These results are consistent with a previous Hg^{2+} detection sensor using the same principle [31]. In addition, to further confirm that the signal decrease is caused by the binding of Hg^{2+} with the Poly-T region in AT11A, another MB (Hg-MB-AA) was synthesized by immobilizing AA (a G-quadruplex motif without a Poly-T region) on the MBs and was used for Hg^{2+} detection. As shown in the ESM, Fig. S4, no apparent absorbance difference can be observed with or without Hg^{2+}, indicating that the inhibition of peroxidase activity of G-quadruplex/hemin in Hg-MBs is indeed caused by Hg^{2+} binding in the Poly-T region.

Hg^{2+} accumulation with Hg-MBs

To evaluate the accumulation ability of Hg-MBs, the samples with different Hg^{2+} concentrations were treated with Hg-MBs and separated with a magnetic rack. The Hg^{2+} concentration in the supernatants was then detected through the same method as described above. The Hg^{2+} concentrations of samples 1 to 6 were 0.2 to 20 μM. Sample C is a control solution in which no Hg^{2+} was added. As shown in Fig. 3, all samples exhibit less absorbance intensity before Hg^{2+} separation except sample C. However, after the Hg-MBs treatment, samples 1, 2, and 3 show nearly the same absorbance intensity as sample C, which indicates that almost all Hg^{2+} were captured by the Hg-MBs and the Hg^{2+} concentration in the supernatants was close to zero. The absorbances of samples 4 and 5 show a distinct increase compared with those without Hg-MB treatment. A lower absorbance can be found in sample 6, and no obvious change can be found after the Hg^{2+} accumulation step. These results imply that Hg-MBs indeed have Hg^{2+} accumulation ability and can be used as separation probes in a Hg^{2+}-containing solution that does not exceed 1 μM.

Selectivity investigation

To verify whether the existence of other metal ions interferes with the detection of Cd^{2+} and Hg^{2+}, our sensor system was challenged with a series of divalent cations, including Mg^{2+}, Ba^{2+}, Ca^{2+}, Mn^{2+}, Ni^{2+}, Co^{2+}, and Zn^{2+}. As shown in Fig. 4A, the reaction solution containing Cd^{2+} obviously responded at a concentration of 100 nM. In addition, the concentrations of other metal ions were increased to 10 μM, and no apparent signal enhancement was observed except for the Hg^{2+} solution at 10 μM. This happens because 10 μM Hg^{2+} has exceeded the accumulation capacity of Hg-MBs(see Fig. 3), and the free Hg^{2+} in solution could cleave the PS substrate [30], leading to the release of OD-1 as the signal transduction element and subsequent signal increase. Figure 4B shows the selectivity of Hg^{2+} detection using Hg-MBs as the recognition probe. Only Hg^{2+} obviously responded as the concentration increased from 0 to 1000 nM. These results indicate that the other foreign metal ions displayed slight and negligible interferences on the constructed sensor system.

Effects of pH and anions

It has been widely reported that the catalytic performances of DNAzymes are significantly affected by pH [33]. In addition, heavy metals are present in diverse forms at different pH values [34]. Therefore, the compatibility of our sensor system with pH was tested in our study. For Cd^{2+} detection, the PS-substrate cleavage reaction was performed under different pH

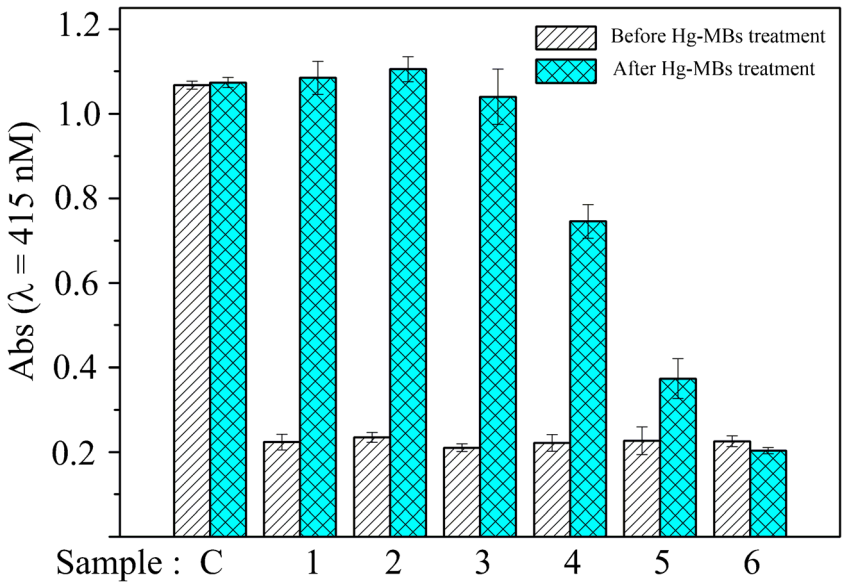

Fig. 3 Absorbance measurement with the Hg^{2+} detection sensor in samples C (0 μM), 1 (0.2 μM), 2 (0.5 μM), 3 (1 μM), 4 (5 μM), 5 (10 μM), and 6 (20 μM) before (**A**) and after (**B**) Hg-MB treatment

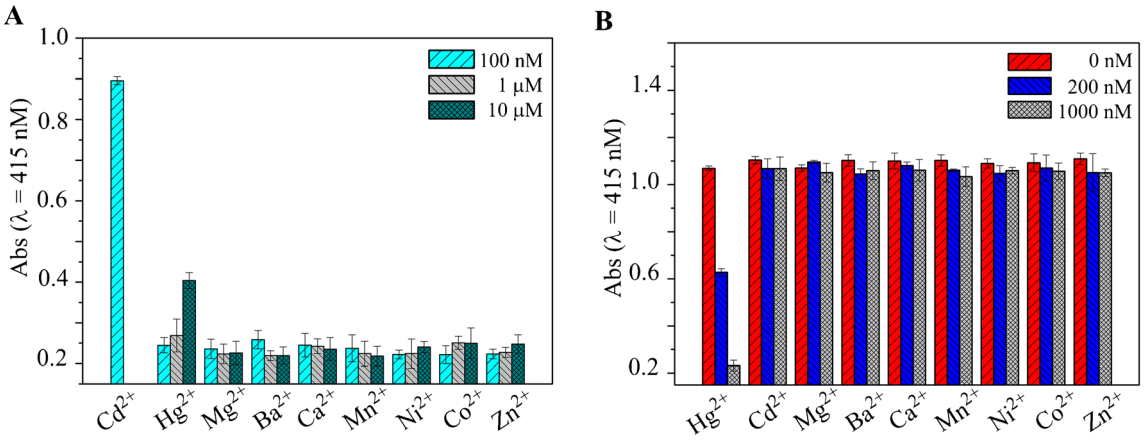

Fig. 4 Specificity of the proposed sensor system for Cd^{2+} (**A**) and Hg^{2+} (**B**) detection. The error bars represent the standard deviation of three repetitive measurements

values, and the absorbances were recorded. As shown in Fig. 5A, higher Ab responses were obtained in weak acid solutions (pH 5 ~ 6), and a slight signal decrease occurred at pH values of approximately 7. The results suggest that the Cd^{2+}-specific DNAzyme in our study is compatible with a wide range of pH values, which is consistent with a recent report [35]. For Hg^{2+} detection, the effect of pH on the G-quadruplex-hemin catalyzed oxidation reaction of ABTS was tested. In the absence of Hg^{2+}, the Abs value decreases with increasing pH, as shown in Fig. 5B, indicating that the G-quadruplex-hemin DNAzyme shows better catalytic activity under acidic conditions [31]. In the presence of Hg^{2+}, the most

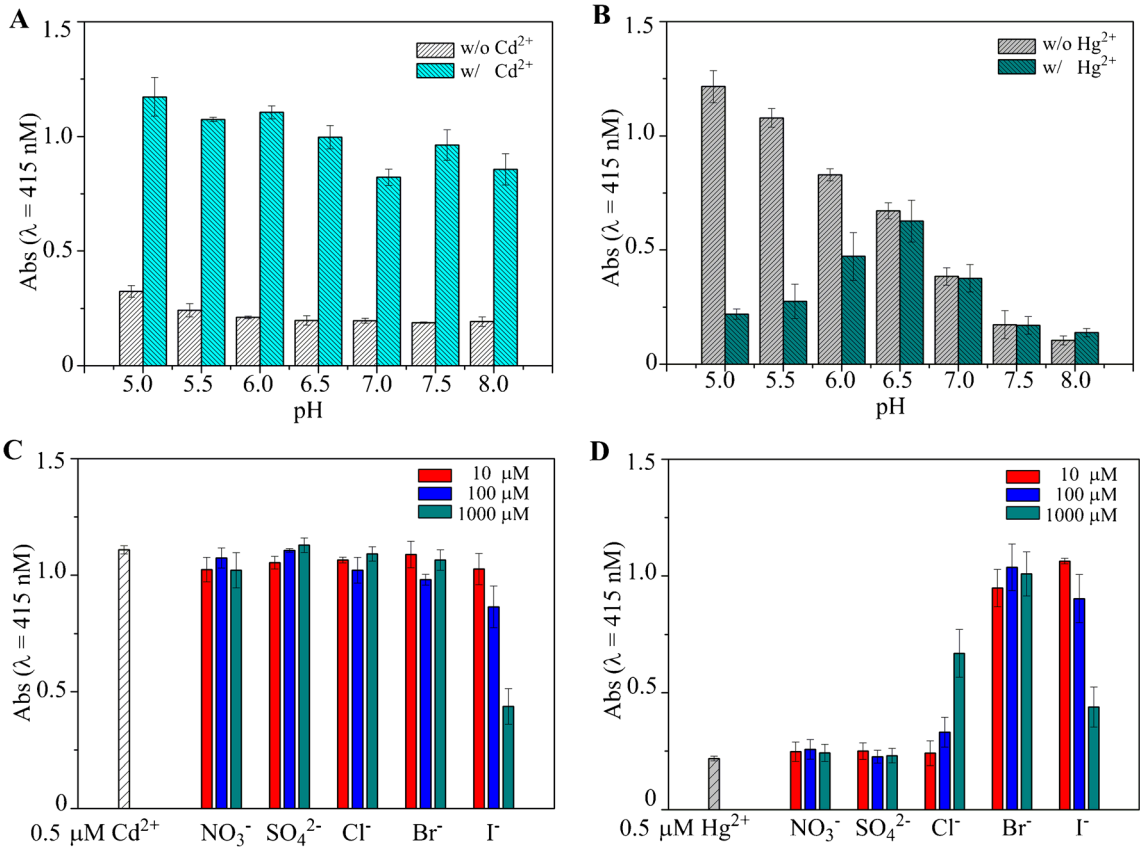

Fig. 5 The effects of pH and anions on the assay. Absorbance was measured with Cd^{2+} (**A**) and Hg^{2+} (**B**) detection sensors at pH 5 ~ 8. Anions at different concentrations (10, 100, and 1000 μM) were added to Cd^{2+} (**C**) and Hg^{2+} (**D**) samples, and the absorption intensity at 415 nm was recorded. The error bars represent the standard deviation of three repetitive measurements

Table 2 Cd^{2+} and Hg^{2+} determination in environmental water samples (n = 6)

Sample	Ions	Found (nM)	Added (nM)	detected (nM)	RSD (%)	Recovery (%)
1[a]	Cd^{2+}	–	50.00	49.88	1.52	99.75
1[a]	Hg^{2+}	–	50.00	50.80	2.45	101.61
2[b]	Cd^{2+}	–	50.00	50.70	1.74	101.39
2[b]	Hg^{2+}	–	50.00	51.01	2.05	102.02
3[c]	Cd^{2+}	–	50.00	50.47	2.60	100.93
3[c]	Hg^{2+}	–	50.00	50.93	3.16	101.85

RSD represents the standard deviation of six repetitive measurements

[a] Tap water

[b] Pond water in Nanjing Forestry University

[c] Xuanwu Lake water

significant signal change was found at pH 5.0. However, a slight and negligible difference was observed when the pH exceeded 6.5 (Fig. 5B). Considering that mercury ions can precipitate under alkaline conditions, a weak signal response may be induced by the lower solubility.

Although anions are repelled by the negatively charged DNA backbone, they may have affinity for target metal ions such as Cd^{2+} and Hg^{2+}, and the sensitivity of DNAzyme could be modulated [36]. The effect of anions (sodium salts of NO_3^-, SO_4^{2-}, Cl^-, Br^-, and I^-) on the assay was tested in our study. As shown in Fig. 5C, no significant signal interference was observed for Cd^{2+} detection after the addition of anions except I^-. We speculated that the reducibility of I^- may affect the G-quadruplex-hemin catalyzed oxidation reaction of ABTS, leading to a decrease in absorbance. On the other hand, Br^- strongly inhibited Hg^{2+} binding with Poly-T in AT11A even at concentrations as low as 10 μM, and the binding inhibition effect of Cl^- emerged at 1000 μM, resulting in an increase in absorbance (Fig. 5D). The solubilities of $HgCl_2$, $HgBr_2$, and HgI_2 in 100 mL water at 20 °C are 6.57 g, 0.56 g, and 0.0062 g, respectively. In addition, their solubility products (K_{sp}) are 2.6×10^{-15}, 6.2×10^{-20}, and 2.9×10^{-29}, respectively [37]. With more than 10 μM anions and 0.5 μM Hg^{2+}, the Br^- sample already reached the K_{sp} value of $HgBr_2$, and only trace amounts of Hg^{2+} were ionized, while the Cl^- samples remained soluble. Although 10 μM I^- is perfectly capable of trapping Hg^{2+} in solution, an excess of I^-(1000 μM) could affect the oxidation reaction of ABTS, leading to a decrease in the signal.

Application in environmental water samples

With the aim of evaluating the analytical reliability and application potential of our sensor system in environmental samples, we examined samples from tap water, pond water at Nanjing Forestry University, and lake water from Nanjing Xuanwu Lake. All samples were filtered with 0.22-μm membrane. The reproducibility of the sensor system was evaluated based on the relative standard deviation (RSD). As shown in Table 2, the recoveries of Cd^{2+} in the three samples are in the range of 99.75 to 101.39%, and the RSD is lower than 2.60%. For Hg^{2+} determination, the recoveries and RSD are in the range of 101.60 to 102.85% and lower than 3.16%, respectively. The results above indicate that the sensor system reported in this work is reliable and could be further used in environmental monitoring.

Conclusion

In summary, a DNAzyme-based colorimetric biosensor assay for the detection of Cd^{2+} and Hg^{2+} in aqueous solutions was developed. Cd^{2+}-dependent DNAzyme cleavage and Hg^{2+} binding in the loop of the G-quadruplex induce a change in the catalytic activity of the G-quadruplex/hemin DNAzyme, along with a dramatic change in the rate of ABTS oxidation and the color in solution. The constructed biosensor assay exhibited excellent selectivity and high sensitivity. In particular, by using an accumulation probe, our biosensor assay for Cd^{2+} detection can rule out false-positive results induced by Hg^{2+} nonspecific substrate cleavage and has better Cd^{2+} response specificity in the multiple heavy metal contamination samples. Furthermore, the assay was used to detect the environmental water samples, and the target recovery results were reasonable, indicating that the sensor system is reliable and could be further used in environmental monitoring.

Supplementary Information The online version contains supplementary material available at https://doi.org/10.1007/s00216-021-03677-x.

Funding This work was supported by the Natural Science Foundation of Jiangsu Province (No. BK20181028), the Startup Foundation (GXL2014038), the Jiangsu Innovative Research Program for Talent from the World's Famous Universities, and the Priority Academic

Program Development (PAPD) program of Jiangsu Province at Nanjing Forestry University. This work was also funded by the Natural Science Foundation of the Jiangsu Higher Education Institutions of China (17KJB150011) and the Startup Foundation (JSNU2016YB02) at Jiangsu Second Normal University.

Declarations

Conflict of interest The authors declare no competing interests.

References

1. Yu Y, Zhou X, Zhu Z, Zhou K. Sodium hydrosulfide mitigates cadmium toxicity by promoting cadmium retention and inhibiting its translocation from roots to shoots in Brassica napus. J Agric Food Chem. 2019;67(1):433–40. https://doi.org/10.1021/acs.jafc.8b04622.
2. Vitkova M, Puschenreiter M, Komarek M. Effect of nano zero-valent iron application on As, Cd, Pb, and Zn availability in the rhizosphere of metal(loid) contaminated soils. Chemosphere. 2018;200:217–26. https://doi.org/10.1016/j.chemosphere.2018.02.118.
3. Wang H, Engstrom AK, Xia Z. Cadmium impairs the survival and proliferation of cultured adult subventricular neural stem cells through activation of the JNK and p38 MAP kinases. Toxicology. 2017;380:30–7.
4. Ma HH, Gao F, Zhang XX, Cui BJ, Liu Y, Li ZY. Formation of iron plaque on roots of Iris pseudacorus and its consequence for cadmium immobilization is impacted by zinc concentration. Ecotox Environ Safe. 2020:193.
5. Zeng H, Tang Y, Zou WY, Wang CX, Tao H, Wu YG. V6O13 nanobelts for simultaneous detection of Cd(II) and Pb(II) in water. Acs Appl Nano Mater. 2021;4(5):4654–64.
6. Zahir F, Rizwi SJ, Haq SK, Khan RH. Low dose mercury toxicity and human health. Environ Toxicol Pharmacol. 2005;20(2):351–60.
7. Garza-Lombo C, Posadas Y, Quintanar L, Gonsebatt ME, Franco R. Neurotoxicity linked to dysfunctional metal ion homeostasis and xenobiotic metal exposure: redox signaling and oxidative stress. Antioxid Redox Signal. 2018;28(18):1669–703.
8. Londonio A, Morzan E, Smichowski P. Determination of toxic and potentially toxic elements in rice and rice-based products by inductively coupled plasma-mass spectrometry. Food Chem. 2019;284:149–54. https://doi.org/10.1016/j.foodchem.2019.01.104.
9. Martinez D, Grindlay G, Gras L, Mora J. Determination of cadmium and lead in wine samples by means of dispersive liquid-liquid microextraction coupled to electrothermal atomic absorption spectrometry. J Food Compos Anal. 2018;67:178–83.
10. Liu J, Cao Z, Lu Y. Functional nucleic acid sensors. Chem Rev. 2009;109(5):1948–98. https://doi.org/10.1021/cr030183i.
11. Lyu C, Khan IM, Wang Z. Capture-SELEX for aptamer selection: a short review. Talanta. 2021;229:122274. https://doi.org/10.1016/j.talanta.2021.122274.
12. Chen JH, Pan JF, Liu CS. Versatile sensing platform for Cd2+ detection in rice samples and its applications in logic gate computation. Anal Chem. 2020;92(8):6173–80.
13. Kiy MM, Zaki A, Menhaj AB, Samadi A, Liu JW. Dissecting the effect of anions on Hg2+ detection using a FRET based DNA probe. Analyst. 2012;137(15):3535–40. https://doi.org/10.1039/c2an35314h.
14. Xiang Y, Tong A, Lu Y. Abasic site-containing DNAzyme and aptamer for label-free fluorescent detection of Pb(2+) and adenosine with high sensitivity, selectivity, and tunable dynamic range. J Am Chem Soc. 2009;131(42):15352–7. https://doi.org/10.1021/ja905854a.
15. Lu ZJ, Wang P, Xiong WW, Qi BP, Shi RJ, Xiang DS, Zhai K. Simultaneous detection of mercury (II), lead (II) and silver (I) based on fluorescently labelled aptamer probes and graphene oxide. Environ Technol. 2020.
16. Mao K, Zhang H, Wang Z, Cao H, Zhang K, Li X, Yang Z. Nanomaterial-based aptamer sensors for arsenic detection. Biosens Bioelectron. 2020;148:111785. https://doi.org/10.1016/j.bios.2019.111785.
17. Xiong M, Yang Z, Lake RJ, Li J, Hong S, Fan H, Zhang XB, Lu Y. DNAzyme-mediated genetically encoded sensors for ratiometric imaging of metal ions in living cells. Angew Chem. 2020;59(5):1891–6. https://doi.org/10.1002/anie.201912514.
18. Wang H, Yin Y, Gang L. Single-gap microelectrode functionalized with single-walled carbon nanotubes and Pbzyme for the determination of Pb2+. Electroanal. 2019;31(6):1174–81.
19. Torabi SF, Lu Y. Identification of the same Na+-specific DNAzyme motif from two in vitro selections under different conditions. J Mol Evol. 2015;81(5–6):225–34.
20. Jiang ZL, Yao DM, Wen GQ, Li TS, Chen B, Liang AH. A label-free nanogold DNAzyme-cleaved surface-enhanced resonance Raman scattering method for trace UO22+ using rhodamine 6G as probe. Plasmonics. 2013;8(2):803–10.
21. Liu SF, Cheng CB, Gong HW, Wang L. Programmable Mg2+-dependent DNAzyme switch by the catalytic hairpin DNA assembly for dual-signal amplification toward homogeneous analysis of protein and DNA. Chem Commun. 2015;51(34):7364–7.
22. Wang H, Liu Y, Liu G. Label-free biosensor using a silver specific RNA-cleaving DNAzyme functionalized single-walled carbon nanotube for silver ion determination. Nanomaterials-Basel. 2018;8(4).
23. Yang D, Cheng W, Chen X, Tang Y, Miao P. Ultrasensitive electrochemical detection of miRNA based on DNA strand displacement polymerization and Ca(2+)-dependent DNAzyme cleavage. Analyst. 2018;143(22):5352–7. https://doi.org/10.1039/c8an01555d.
24. Liu J, Lu Y. Colorimetric Cu2+ detection with a ligation DNAzyme and nanoparticles. Chem Commun. 2007;46:4872–4. https://doi.org/10.1039/b712421j.
25. Zhou W, Vazin M, Yu T, Ding J, Liu J. In vitro selection of chromium-dependent DNAzymes for sensing chromium(III) and chromium(VI). Chemistry. 2016;22(28):9835–40. https://doi.org/10.1002/chem.201601426.
26. Huang PJ, Liu J. Rational evolution of Cd2+−specific DNAzymes with phosphorothioate modified cleavage junction and Cd2+ sensing. Nucleic Acids Res. 2015;43(12):6125–33. https://doi.org/10.1093/nar/gkv519.
27. Wang H, Liu Y, Liu G. Electrochemical biosensor using DNA embedded phosphorothioate modified RNA for mercury ion determination. Acs Sensors. 2018;3(3):624–31.
28. Huang PJJ, Liu JW. Sensing parts-per-trillion Cd2+, Hg2+, and Pb2+ collectively and individually using phosphorothioate DNAzymes. Anal Chem. 2014;86(12):5999–6005.
29. Wang H, Zheng SS, Nan XM, Zhao YG, Wang Y, Zhang F, Yang L, Xu LX, Xiong BH (2021)Non-specific DNAzyme-based biosensor with interfering ions for the Cd2+ determination in feed. Sensor Actuat B-Chem 329.
30. Huang PJJ, Wang F, Liu JW. Cleavable molecular beacon for Hg2+ detection based on phosphorothioate RNA modifications. Anal Chem. 2015;87(13):6890–5.
31. Gao HL, Zhao JX, Huang Y, Cheng X, Wang S, Han Y, Xiao Y, Lou XH. Universal design of structure-switching aptamers with signal reporting functionality. Anal Chem. 2019;91(22):14514–21.

32. Burge S, Parkinson GN, Hazel P, Todd AK, Neidle S. Quadruplex DNA: sequence, topology and structure. Nucleic Acids Res. 2006;34(19):5402–15. https://doi.org/10.1093/Nar/Gkl655.
33. Li T, Li B, Wang E, Dong S. G-quadruplex-based DNAzyme for sensitive mercury detection with the naked eye. Chem Commun. 2009;24:3551–3. https://doi.org/10.1039/b903993g.
34. Jackson VE, Felmy AR, Dixon DA. Prediction of the pKa's of aqueous metal ion +2 complexes. J Phys Chem A. 2015;119(12): 2926–39. https://doi.org/10.1021/jp5118272.
35. Wang G, Wu M, Chu LT, Chen TH. Portable microfluidic device with thermometer-like display for real-time visual quantitation of cadmium(II) contamination in drinking water. Anal Chim Acta. 2021;1160:338444. https://doi.org/10.1016/j.aca.2021.338444.
36. Ren W, Huang PJ, He M, Lyu M, Wang C, Wang S, Liu J. Sensitivity of a classic DNAzyme for Pb(2+) modulated by cations, anions and buffers. Analyst. 2020;145(4):1384–8. https://doi.org/10.1039/c9an02612f.
37. Speight JG (2017) Lange's handbook of chemistry. McGraw-Hill Education,